

# A Feasible Reduced Space Method for Real-Time Optimal Power Flow

François Pacaud, Daniel Adrian Maldonado, Sungho Shin, Michel Schanen, Mihai Anitescu Mathematics and  
Computer Science Department  
Argonne National Laboratory  
Lemont, U.S.A  
{fpacaud,maldonadod,sshin,mschanen,anitescu}@anl.gov

**Abstract**—We propose a novel feasible-path algorithm to solve the optimal power flow (OPF) problem for real-time use cases. The method augments the seminal work of Dommel and Tinney with second-order derivatives to work directly in the reduced space induced by the power flow equations. In the reduced space, the optimization problem includes only inequality constraints corresponding to the operational constraints. While the reduced formulation directly enforces the physical constraints, the operational constraints are softly enforced through Augmented Lagrangian penalty terms. In contrast to interior-point algorithms (state-of-the-art for solving OPF), our algorithm maintains feasibility at each iteration, which makes it suitable for real-time application. By exploiting accelerator hardware (Graphic Processing Units) to compute the reduced Hessian, we show that the second-order method is numerically tractable and is effective to solve both static and real-time OPF problems.

**Index Terms**—OPF, Reduced-Space, Feasible method

## I. INTRODUCTION

With the increasing penetration of rapidly varying renewable generation resources and electrical vehicles, there is a growing need to compute the generation dispatch at much higher time frequency. This requires adaptation of optimal power flow (OPF) algorithms for operation in a real-time setting. Here, finding the optimum becomes secondary comparing to finding a feasible solution within a tight time constraint [1]. In addition, state-of-the-art OPF algorithms are mature tools on a slow timescale, but they are not adapted to operate in a real-time setting. Generally, the intermediate iterates do not satisfy the power flow equations — encoding the physical constraints (PCs) of the network — and the solution is not realizable before the algorithm has converged. Novel real-time OPF approaches try to remedy this issue and track closely the network changes, at a faster timescale [2], [3], [4], [5].

The reduced space algorithm of Dommel and Tinney [6] is a promising candidate for these real-time applications. By design, it works directly in the manifold induced by the power flow equations, so all iterates inherently satisfy the PCs. The operational constraints (OCs) are enforced with soft penalties, commonly used in real-time optimization to avoid expensive active-set reordering operations [2], [4], [7], [8]. However, the algorithm has fallen out of favor in the 1980s, with the advent of interior point algorithms (see [9] for a survey). This is due to practical limitations of the algorithm: (1) the iterates are updated in the reduced-space using only first-order information, impairing the speed of convergence of the

algorithm. (2) the large number of OCs in the problem limits the available degrees of freedom in the reduced space. We refer to the recent report of Kardos et al. [10] for further details on the limitations of the algorithm.

This article revisits the reduced space algorithm [6] in a real-time optimization setting while addressing (1) and (2). (1) We efficiently extract the reduced Hessian in the reduced space, by leveraging GPUs with automatic differentiation (AD) and by parallelizing the code. The GPUs enable fast computation of second-order information to compute the descent direction in the reduced space. (2) We propose an augmented Lagrangian (AL) formulation to reformulate the OCs with smooth penalty terms (PCs being satisfied by design). First, this allows to devise a practical AL algorithm to solve the *static OPF* in the reduced space, with a tractable running time. Second, we can exploit the AL formulation to track the solution found previously by the static OPF algorithm, in a real-time setting. Our *real-time OPF* algorithm explicitly exploits the reduced Hessian to update the tracking control. Previous real-time algorithms [2], [4] only rely on first-order information (with a projected gradient or a LBFGS algorithm). Numerical results show that the method efficiently tracks a suboptimal solution on instances with up to 9241 buses.

In Section II, we introduce the OPF problem before presenting in Section III the reduced space problem with the expressions of the gradient and the Hessian in the reduced space. In Section IV, we develop two algorithms based on an AL formulation to solve static and real-time OPF problems. Finally, we show in Section V that the two algorithms are numerically tractable by solving large-scale OPF instances.

## A. Notation

All vectors are noted in bold  $\mathbf{x} = (x_1, \dots, x_n) \in \mathbb{R}^n$ .  $\|\cdot\|$  and  $\|\cdot\|$  :  $\mathbb{R}^n \rightarrow \mathbb{R}^{n \times n}$  denote the Euclidean norm and the diagonal operator, respectively. For any variable  $x$ , its lower bound is denoted by  $x^b$ , its upper bound by  $x^\#$ . Finally,  $d$  denotes the differential operator,  $d_x(\cdot)$  the total derivative  $\frac{d(\cdot)}{dx}$ , and  $\partial_x(\cdot)$  the partial derivative  $\frac{\partial(\cdot)}{\partial x}$ . Consistent with the Jacobian's definition, the gradient is defined as the *row* vector  $\nabla_x(\cdot) = (\partial_{x_1}(\cdot), \dots, \partial_{x_n}(\cdot)) \in \mathbb{R}^{1 \times n}$ , and is thus assimilated into the total derivative.

## II. MODEL AND FORMULATION

This section introduces an alternate current optimal power flow model (AC-OPF) associated with a transmission grid.

### A. Optimal power flow

We use the most widely used polar formulation [11] as our model. Let a power grid with  $n_b$  buses,  $n_g$  generators and  $n_\ell$  lines. We denote by  $\mathbf{v}, \boldsymbol{\theta} \in \mathbb{R}^{n_b}$  the voltage magnitudes and the voltage angles at each bus. The active and reactive power generations are denoted respectively by  $\mathbf{p}^g, \mathbf{q}^g \in \mathbb{R}^{n_g}$ , and the active and reactive loads by  $\mathbf{p}^d, \mathbf{q}^d$ .

At fixed loads  $(\mathbf{p}^d, \mathbf{q}^d)$ , the optimal power flow aims at finding an operational point  $(\mathbf{v}, \boldsymbol{\theta}, \mathbf{p}^g, \mathbf{q}^g)$  that minimizes the active power generation cost while satisfying the physical and the operational constraints of the network. We get the ACOFP problem written in polar form:

$$\min_{\mathbf{v}, \boldsymbol{\theta}, \mathbf{p}, \mathbf{q}} \sum_{i=1}^{n_g} c_{i,1}^g (p_i)^2 + c_{i,2}^g (p_i) + c_{i,3}^g \quad (1a)$$

$$\text{subject to } G(\mathbf{v}, \boldsymbol{\theta}, \mathbf{p}, \mathbf{q}) = 0 \quad H(\mathbf{v}, \boldsymbol{\theta}) \leq \mathbf{h}^\#, \quad (1b)$$

$$\mathbf{v}^b \leq \mathbf{v} \leq \mathbf{v}^\#, \quad \boldsymbol{\theta}_{ref} = 0, \quad (1c)$$

$$\mathbf{p}^b \leq \mathbf{p} \leq \mathbf{p}^\#, \quad \mathbf{q}^b \leq \mathbf{q} \leq \mathbf{q}^\#. \quad (1d)$$

The quadratic objective (1a) depends only on the active power generation, with coefficients  $c_1^g, c_2^g, c_3^g \in \mathbb{R}^{n_g}$  specifying the cost of each generator. In (1b), the equality constraint  $G$  encodes the  $2 \times n_b$  complete power balance equations and the inequality constraint  $H$  encodes the  $2 \times n_\ell$  line flow limits. The bounds (1c)-(1d) ensure that the voltage magnitudes and the power generations satisfy their operational limits.

### B. State and control variables

In the power flow, the buses are classified into three categories: REF (or slack bus), PV (or generator buses), and PQ (or load buses). We define the *control* variable  $\mathbf{u}$  by gathering the voltage magnitudes at the PV buses and at the slack, as well as the active power generation at PV buses. Similarly, we define a *state* variable  $\mathbf{x}$  with the voltage magnitudes at PQ buses and the voltage angles at PQ and PV buses. We get:

$$\mathbf{u} = (\mathbf{v}_{ref}, \mathbf{v}_{pv}, \mathbf{p}_{pv}^g), \quad \mathbf{x} = (\boldsymbol{\theta}_{pv}, \boldsymbol{\theta}_{pq}, \mathbf{v}_{pq}). \quad (2)$$

If the control  $\mathbf{u}$  is fixed, the state  $\mathbf{x}$  is entirely determined by a subset of the power flow equations  $G$ , denoted here by the function  $g: \mathbb{R}^{n_x} \times \mathbb{R}^{n_u} \rightarrow \mathbb{R}^{n_x}$  [12].

Hence, we can derive a new OPF formulation depending only on the state  $\mathbf{x}$  and the control  $\mathbf{u}$ . We define the functions  $h(\mathbf{x}, \mathbf{u}) = H(\mathbf{v}, \boldsymbol{\theta})$  for line constraints, and  $r(\mathbf{x}, \mathbf{u}) = (\mathbf{v}_{pq}, \mathbf{p}_{ref}^g, \mathbf{q}_{ref}^{net}, \mathbf{q}_{pv}^{net}) \in \mathbb{R}^{n_{pq} + 2n_{ref} + n_{pv}}$  to gather the remaining operational constraints (voltage angles are unconstrained), yielding the problem

$$\begin{aligned} \min_{\mathbf{x}, \mathbf{u}} \quad & f(\mathbf{x}, \mathbf{u}) \\ \text{subject to} \quad & \mathbf{u}^b \leq \mathbf{u} \leq \mathbf{u}^\#, \quad g(\mathbf{x}, \mathbf{u}) = 0, \\ & \mathbf{r}^b \leq r(\mathbf{x}, \mathbf{u}) \leq \mathbf{r}^\#, \quad h(\mathbf{x}, \mathbf{u}) \leq \mathbf{h}^\#, \end{aligned} \quad (3)$$

with  $\mathbf{r}^b = (\mathbf{v}_{pq}^b, \mathbf{p}_{ref}^{g,b}, \mathbf{q}_{ref}^{g,b}, C_g^{pv} \mathbf{q}_{pv}^{g,b})$  and  $\mathbf{r}^\# = (\mathbf{v}_{pq}^\#, \mathbf{p}_{ref}^{g,\#}, \mathbf{q}_{ref}^{g,\#}, C_g^{pv} \mathbf{q}_{pv}^{g,\#})$  (by convention the slack bus has only one generator).  $C_g \in \mathbb{R}^{n_b \times n_g}$  is the bus-generator incidence matrix. In (3), we have a total of  $m = 2n_\ell + n_{pq} + n_{pv} + 2$  nonlinear constraints.

Note that problem (3) is not equivalent to the original OPF (1), as we are not controlling explicitly the reactive power generations (we only bound the net power injections in the functional  $r(\mathbf{x}, \mathbf{u})$ ). That means that if we have multiple generators associated with the same bus, we cannot recover the individual reactive power generations for each generator from a couple  $(\mathbf{x}, \mathbf{u})$ . However, when compared to the structure of (1), (3) allows us to significantly reduce the dimension of the problem. We will explain in the next section the basis of the reduced space method.

## III. REDUCED SPACE PROBLEM

Section II introduced the OPF problem, parameterized by a state  $\mathbf{x}$  and a control  $\mathbf{u}$ . In Section III-A, we exploit the implicit relation between the control  $\mathbf{u}$  and the state  $\mathbf{x}$  to build a reduced space problem, depending *only* on the control  $\mathbf{u}$ . Then, we derive in Section III-B the reduced gradient and the reduced Hessian using the adjoint and the adjoint-adjoint methods, respectively.

### A. Reduced space

The functional  $g$  encoding the  $n_x$  power flow equations is continuously differentiable. By the Implicit Function theorem, it follows that if the Jacobian  $\nabla_x g(\cdot, \mathbf{u})$  is invertible at a given control  $\mathbf{u}$ , then there exists a local function  $x: \mathbb{R}^{n_u} \rightarrow \mathbb{R}^{n_x}$  such that  $g(x(\mathbf{u}), \mathbf{u}) = 0$  locally.

a) *Resolution of power flow equations:* At a fixed control  $\mathbf{u}$ , the nonlinear equations  $g(\mathbf{x}, \mathbf{u}) = 0$  are solved using a Newton-Raphson algorithm [12]. Starting at an initial guess  $\mathbf{x}^{(0)}$ , the algorithm computes the solution  $\mathbf{x}^*(\mathbf{u})$  through

$$\mathbf{x}_{k+1} = \mathbf{x}_k - (\nabla_x g_k)^{-1} \mathbf{g}_k. \quad (4)$$

b) *Reduced space OPF:* Applying the Implicit Function theorem, we eliminate all equality constraints in (3) and we get the reduced space problem with remaining control variables  $\mathbf{u}$ :

$$\begin{aligned} \min_{\mathbf{u}^b \leq \mathbf{u} \leq \mathbf{u}^\#} \quad & f(\mathbf{x}(\mathbf{u}), \mathbf{u}) \\ \text{subject to} \quad & h(\mathbf{x}(\mathbf{u}), \mathbf{u}) \leq \mathbf{h}^\#, \quad \mathbf{r}^b \leq r(\mathbf{x}(\mathbf{u}), \mathbf{u}) \leq \mathbf{r}^\#. \end{aligned} \quad (5)$$

Problem (5) is equivalent to (3), but has a smaller dimension ( $n_u$  instead of  $n_u + n_x$ ). This implies solving the power flow equations for all trial points  $\mathbf{u}$ , and requires expensive (but highly parallelizable) computations for the reduced gradient and the reduced Hessian (see Section III-B).

### B. Reduced sensitivities

1) *Reduced gradient:* If we use the chain rule to differentiate the objective in (5), we get  $\nabla_{\mathbf{u}} f = \partial_{\mathbf{u}} f + \partial_{\mathbf{x}} f \cdot \nabla_{\mathbf{u}} \mathbf{x}$ . However, this expression is expensive to evaluate, as the Jacobian  $\nabla_{\mathbf{u}} \mathbf{x}$  (also called *sensitivity matrix*) is a dense matrix with dimension  $n_x \times n_u$ . Instead, we evaluate the reduced gradient with the *adjoint method*.

**Proposition 1** (Adjoint method). *Let  $(\mathbf{x}, \mathbf{u}) \in \mathbb{R}^{n_x} \times \mathbb{R}^{n_u}$  such that  $g(\mathbf{x}, \mathbf{u}) = 0$ , and a first-order adjoint  $\boldsymbol{\lambda} \in \mathbb{R}^{n_x}$  solution of the linear system  $(\nabla_{\mathbf{x}}g)^\top \boldsymbol{\lambda} = -(\partial_{\mathbf{x}}f)^\top$ . Then, the reduced gradient satisfies*

$$\nabla_{\mathbf{u}}f = \partial_{\mathbf{u}}f + \boldsymbol{\lambda}^\top \cdot \nabla_{\mathbf{u}}g. \quad (6)$$

*Proof.* Let  $(\mathbf{x}, \mathbf{u}) \in \mathbb{R}^{n_x} \times \mathbb{R}^{n_u}$  such that  $g(\mathbf{x}, \mathbf{u}) = 0$ . For all  $\boldsymbol{\lambda} \in \mathbb{R}^{n_x}$ , we define the Lagrangian

$$\ell(\mathbf{x}, \mathbf{u}, \boldsymbol{\lambda}) := f(\mathbf{x}, \mathbf{u}) + \boldsymbol{\lambda}^\top g(\mathbf{x}, \mathbf{u}). \quad (7)$$

As  $g(\mathbf{x}, \mathbf{u}) = 0$ , the Lagrangian  $\ell(\mathbf{x}, \mathbf{u}, \boldsymbol{\lambda})$  does not depend on  $\boldsymbol{\lambda}$  and we have  $\ell(\mathbf{x}, \mathbf{u}, \boldsymbol{\lambda}) = f(\mathbf{x}, \mathbf{u})$ . Applying the chain-rule, leads to the total derivative of  $\ell$  w.r.t.  $\mathbf{u}$

$$\begin{aligned} d_{\mathbf{u}}\ell &= (\partial_{\mathbf{x}}f \cdot \nabla_{\mathbf{u}}\mathbf{x} + \partial_{\mathbf{u}}f) + \boldsymbol{\lambda}^\top (\nabla_{\mathbf{x}}g \cdot \nabla_{\mathbf{u}}\mathbf{x} + \nabla_{\mathbf{u}}g) \\ &= (\partial_{\mathbf{u}}f + \boldsymbol{\lambda}^\top \nabla_{\mathbf{u}}g) + (\partial_{\mathbf{x}}f + \boldsymbol{\lambda}^\top \nabla_{\mathbf{x}}g) \nabla_{\mathbf{u}}\mathbf{x}. \end{aligned}$$

Fixing  $\boldsymbol{\lambda} = -(\nabla_{\mathbf{x}}g)^{-\top} (\partial_{\mathbf{x}}f)^\top$ , eliminates the dependency w.r.t.  $\nabla_{\mathbf{u}}\mathbf{x}$  and we get the expression in (6).  $\square$

2) *Reduced Hessian:* By analogy to Proposition 1, we derive the adjoint-adjoint method [13], which instead of using the nonlinear equations  $g(\mathbf{x}, \mathbf{u}) = 0$ , considers the extended nonlinear system

$$\begin{cases} g(\mathbf{x}, \mathbf{u}) = 0 \\ \partial_{\mathbf{x}}f(\mathbf{x}, \mathbf{u}) + \boldsymbol{\lambda}^\top \nabla_{\mathbf{x}}g(\mathbf{x}, \mathbf{u}) = 0, \end{cases} \quad (8)$$

(the second line is null by definition of the first-order adjoint  $\boldsymbol{\lambda}$  in Proposition 1). By associating two adjoints  $\mathbf{z}, \boldsymbol{\psi}$  to the two equations (8), the adjoint-adjoint method amounts to the Hessian-vector product  $(\nabla^2 f)\mathbf{w}$ ,  $\mathbf{w} \in \mathbb{R}^{n_u}$ .

**Proposition 2** (Adjoint-adjoint method [13]). *Let  $(\mathbf{x}, \mathbf{u}, \boldsymbol{\lambda}) \in \mathbb{R}^{n_x} \times \mathbb{R}^{n_u} \times \mathbb{R}^{n_x}$  such that (8) is satisfied, and  $\mathbf{w} \in \mathbb{R}^{n_u}$  any real vector. Then, the reduced Hessian-vector product is equal to*

$$(\nabla^2 f)\mathbf{w} = (\nabla_{\mathbf{u}\mathbf{u}}^2 \ell)\mathbf{w} + (\nabla_{\mathbf{u}\mathbf{x}}^2 \ell)^\top \mathbf{z} + (\nabla_{\mathbf{u}}g)^\top \boldsymbol{\psi}. \quad (9)$$

where the two second-order adjoints  $(\mathbf{z}, \boldsymbol{\psi}) \in \mathbb{R}^{n_x} \times \mathbb{R}^{n_x}$  are defined as solutions of the two linear systems:

$$\begin{cases} (\nabla_{\mathbf{x}}g) \mathbf{z} = -\nabla_{\mathbf{u}}g \cdot \mathbf{w} \\ (\nabla_{\mathbf{x}}g)^\top \boldsymbol{\psi} = -(\nabla_{\mathbf{x}\mathbf{u}}^2 \ell)\mathbf{w} - (\nabla_{\mathbf{x}\mathbf{x}}^2 \ell)\mathbf{z}. \end{cases} \quad (10)$$

*Proof.* Let  $\hat{g}(\mathbf{x}, \mathbf{u}, \boldsymbol{\lambda}) := \partial_{\mathbf{x}}f(\mathbf{x}, \mathbf{u}) + \boldsymbol{\lambda}^\top \nabla_{\mathbf{x}}g(\mathbf{x}, \mathbf{u})$ . We define a new Lagrangian  $\hat{\ell}$  associated withby introducing two second-order adjoints  $\mathbf{z}, \boldsymbol{\psi} \in \mathbb{R}^{n_x}$ :

$$\hat{\ell}(\mathbf{x}, \mathbf{u}, \mathbf{w}, \boldsymbol{\lambda}; \mathbf{z}, \boldsymbol{\psi}) := (\nabla_{\mathbf{u}}\ell)^\top \mathbf{w} + \mathbf{z}^\top g(\mathbf{x}, \mathbf{u}) + \boldsymbol{\psi}^\top \hat{g}(\mathbf{x}, \mathbf{u}, \boldsymbol{\lambda}).$$

When (8) is satisfied,  $\hat{\ell}$  does not depend on  $\mathbf{z}$  and  $\boldsymbol{\psi}$ . By deriving  $\hat{\ell}$  and choosing  $(\mathbf{z}, \boldsymbol{\psi})$  solutions of the two linear systems (10), we get the expression (9).  $\square$

As  $\nabla^2 \ell = \nabla^2 f + \boldsymbol{\lambda}^\top \nabla^2 g$ , we observe that both Equations (9) and (10) involve the third-order tensors  $\nabla_{\mathbf{x}\mathbf{x}}^2 g$ ,  $\nabla_{\mathbf{x}\mathbf{u}}^2 g$ , and  $\nabla_{\mathbf{u}\mathbf{u}}^2 g$ . We will see in the next subsection that in practice we do not need to evaluate the three tensors explicitly.

### C. Reduced callbacks

We have introduced in Sections III-A and III-B all the elements to compute the callbacks for the reduced space problem (5).

a) *Objective and constraints:* Evaluating the objective  $f(\mathbf{x}(\mathbf{u}), \mathbf{u})$  and the constraints  $h(\mathbf{x}(\mathbf{u}), \mathbf{u})$  requires the evaluation of  $\mathbf{x}(\mathbf{u})$  with the Newton-Raphson algorithm (4). Typically, the algorithm converges in a few iterations. At iteration  $k$ , the algorithm amounts to (i) evaluate the sparse Jacobian  $\nabla_{\mathbf{x}}g_k = \nabla_{\mathbf{x}}g(\mathbf{x}_k, \mathbf{u})$  (ii) solve the linear system  $(\nabla_{\mathbf{x}}g_k)\mathbf{d}_k = -\mathbf{g}_k$  to find the descent direction  $\mathbf{d}_k$ . In step (i), we evaluate the sparse Jacobian  $\nabla_{\mathbf{x}}g_k$  using forward-mode automatic differentiation. In step (ii), we can use any sparse linear solver.

b) *Reduced gradient and Jacobian:* The reduced gradient  $\nabla_{\mathbf{u}}f$  requires the evaluation of the gradients  $\partial_{\mathbf{x}}f, \partial_{\mathbf{u}}f$  and the Jacobian  $\nabla_{\mathbf{u}}g$ . The former are evaluated with manual adjoint differentiation, the latter with forward-mode automatic differentiation. The linear system  $(\nabla_{\mathbf{x}}g)^\top \boldsymbol{\lambda} = -(\partial_{\mathbf{x}}f)^\top$  is solved with the sparse linear solver used in the power flow algorithm (same matrix, but transposed). Similarly, we evaluate the reduced Jacobians  $(\nabla_{\mathbf{u}}h, \nabla_{\mathbf{u}}r)$ , except that it requires solving  $m$  linear systems to evaluate the intermediate adjoints  $\boldsymbol{\mu}_i$ , with, for all  $i = 1, \dots, m$ :  $(\nabla_{\mathbf{x}}g)^\top \boldsymbol{\mu}_i = -(\partial_{\mathbf{x}}h_i)^\top$ .

c) *Reduced Hessian:* The reduced Hessian of the objective  $\nabla^2 f$  is evaluated with the adjoint-adjoint method, using  $n_u$  Hessian-vector products  $\nabla^2 f \cdot \mathbf{e}_i$  (with  $\mathbf{e}_i$  the  $i$ -th Cartesian basis vector). In (9), we avoid evaluating explicitly the tensors  $\nabla_{\mathbf{x}\mathbf{x}}^2 g$ ,  $\nabla_{\mathbf{x}\mathbf{u}}^2 g$ , and  $\nabla_{\mathbf{u}\mathbf{u}}^2 g$  by computing inplace the forward-over-reverse projection  $\sum_{i=1}^{n_x} \lambda_i (\nabla^2 g_i)\mathbf{w}$ . In total, the dense reduced Hessian  $\nabla^2 f$  requires solving  $2n_u$  sparse linear systems, while factorizing both sparse matrices in (10) only once.

However, evaluating the Hessian of the constraints  $\nabla_{\mathbf{u}\mathbf{u}}^2 h$  is generally not tractable. The adjoint-adjoint procedure (see Proposition 2) would be repeated for each first-order adjoint  $\boldsymbol{\mu}_i$ , with  $i = 1, \dots, m$  and would involved solving  $2n_u \times m$  linear systems. In the next section, we will reformulate all operational constraints as soft AL penalties. By doing so, we will only need to evaluate the reduced Hessian of the AL functional.

## IV. RESOLUTION ALGORITHMS

In the previous section, we have devised a method to compute the reduced gradient, the reduced Jacobian and the reduced Hessian of the reduced space problem (5). In IV-A, we reformulate the reduced space problem with an AL formulation. We exploit the AL formulation to design two algorithms, both working in the reduced space. The first algorithm, introduced in Section IV-B, solves the static OPF with an AL algorithm. The second algorithm, in Section IV-C, is able to track the solution of a real-time OPF problem.

### A. Augmented Lagrangian formulation

In what follows, we gather all inequalities in a single functional  $c : \mathbb{R}^{n_u} \rightarrow \mathbb{R}^m$ :  $\mathbf{s}^b \leq c(\mathbf{u}) \leq \mathbf{s}^\sharp$ , with  $c(\mathbf{u}) = (h(\mathbf{u}), r(\mathbf{u}))$ ,  $\mathbf{s}^b = (\mathbf{0}_{2n_l}, \mathbf{r}^b)$  and  $\mathbf{s}^\sharp = (\mathbf{h}^\sharp, \mathbf{r}^\sharp)$ . We rewrite

Problem (5) in standard form by introducing a slack vector  $\mathbf{s}^b \leq \mathbf{s} \leq \mathbf{s}^\sharp$  satisfying  $c(\mathbf{u}) - \mathbf{s} = 0$ :

$$\min_{\substack{\mathbf{u}^b \leq \mathbf{u} \leq \mathbf{u}^\sharp, \\ \mathbf{s}^b \leq \mathbf{s} \leq \mathbf{s}^\sharp}} f(\mathbf{u}) \quad \text{subject to} \quad c(\mathbf{u}) - \mathbf{s} = 0. \quad (11)$$

Problem (11) can be solved with an interior-point method (IPM). However, the evaluation of the Hessian of the Lagrangian requires the resolution of  $(m+1) \times (2n_u+1)$  linear systems (see Section III-C), which is quickly prohibitive. To alleviate this, both Quasi-Newton and constraint aggregation schemes can be used, so far with mixed results. We refer to [10] for a detailed discussion about the resolution of the reduced problem (11) with IPM.

By contrast, by moving all inequality constraints into the objective, an AL formulation requires the resolution of only  $(2n_u+1)$  linear systems to evaluate the full reduced Hessian. For a given penalty  $\rho > 0$  and multiplier vector  $\mathbf{y} \in \mathbb{R}^m$ , the AL subproblem associated with Problem (11) states

$$\min_{\substack{\mathbf{u}^b \leq \mathbf{u} \leq \mathbf{u}^\sharp, \\ \mathbf{s}^b \leq \mathbf{s} \leq \mathbf{s}^\sharp}} f(\mathbf{u}) + \mathbf{y}^\top (c(\mathbf{u}) - \mathbf{s}) + \frac{\rho}{2} \|c(\mathbf{u}) - \mathbf{s}\|^2. \quad (12)$$

Note that introducing the slack variable  $\mathbf{s}$  increases the dimension of the problem from  $n_u$  to  $n_u + m$ , with  $m$  potentially a large number. However, it is well known that the slack variable depends implicitly on the control  $\mathbf{u}$  [14], [15]. Unfortunately, removing the slack  $\mathbf{s}$  in (12) leads to an optimization problem with discontinuous second-order derivatives, impairing the solution algorithm. To avoid this, we exploit instead the structure of the KKT system and show that the slack descent direction  $\mathbf{d}_s$  depends linearly on the control descent direction  $\mathbf{d}_u$ .

1) *Callbacks*: we define the AL functional as:  $L_\rho(\mathbf{u}, \mathbf{s}; \mathbf{y}) = f(\mathbf{u}) + \mathbf{y}^\top (c(\mathbf{u}) - \mathbf{s}) + \frac{\rho}{2} \|c(\mathbf{u}) - \mathbf{s}\|^2$  yielding

$$\begin{cases} \nabla_{\mathbf{u}} L_\rho(\cdot) = \nabla_{\mathbf{u}} f(\mathbf{u}) + (\mathbf{y} + \rho(c(\mathbf{u}) - \mathbf{s}))^\top \nabla_{\mathbf{u}} c(\mathbf{u}) \\ \nabla_{\mathbf{s}} L_\rho(\cdot) = -(\mathbf{y} + \rho(c(\mathbf{u}) - \mathbf{s}))^\top. \end{cases} \quad (13)$$

We note that evaluating the gradient of the AL problem involves the reduced gradient  $\nabla_{\mathbf{u}} f$  and a Jacobian-transpose vector product  $\mathbf{v}^\top \nabla_{\mathbf{u}} c$  (both efficiently computed with our adjoint implementation).

By differentiating again (13), we get the Hessian of the AL functional:

$$\nabla^2 L_\rho = \begin{bmatrix} H_{\mathbf{u}\mathbf{u}} + \rho(\nabla_{\mathbf{u}} c)^\top \nabla_{\mathbf{u}} c & -\rho(\nabla_{\mathbf{u}} c)^\top \\ -\rho \nabla_{\mathbf{u}} c & \rho I \end{bmatrix}, \quad (14)$$

where  $H_{\mathbf{u}\mathbf{u}} = \nabla^2 f(\mathbf{u}) + \sum_{i=1}^m (y_i + \rho(c_i(\mathbf{u}) - s_i)) \nabla^2 c_i(\mathbf{u})$ .

2) *Scaling*: In our implementation, we have to scale the problem to ensure that the order of magnitude of the objective matches those of the different constraints (and thus avoid any degeneracy). The scaling of the objective  $\sigma_f \in \mathbb{R}$  and the scaling of the constraints  $\sigma_c \in \mathbb{R}^m$  can be heuristically estimated, or by scaling the constraints with the absolute norm of their gradient [16], [17]. By noting  $D_c = \llbracket \sigma_c \rrbracket$ , the scaled AL problem writes out:

$$\min_{\substack{\mathbf{u}^b \leq \mathbf{u} \leq \mathbf{u}^\sharp, \\ \mathbf{s}^b \leq \mathbf{s} \leq \mathbf{s}^\sharp}} \sigma_f \cdot f(\mathbf{u}) + \mathbf{y}^\top \cdot D_c (c(\mathbf{u}) - \mathbf{s}) + \frac{\rho}{2} \|D_c (c(\mathbf{u}) - \mathbf{s})\|^2.$$

## B. Static optimal power flow

The static OPF amounts to solving (11) with an AL algorithm.

1) *Solving the Augmented Lagrangian's subproblems*: Starting from initial primal-dual variables  $(\mathbf{u}_0, \mathbf{s}_0; \mathbf{y}_0)$ , the algorithm solves at each iteration (12) to a given tolerance, for a fixed penalty  $\rho$  and multiplier vector  $\mathbf{y}$ .

Here, we solve each subproblem (12) with an IPM. Even if IPMs lack the inherent warmstart capability of active-set methods [18], they do not require reordering of the Hessian matrix; expensive on GPUs.

We note  $\mathbf{w} := (\mathbf{u}, \mathbf{s}) \in \mathbb{R}^{n_u+m}$  the primal variable, and  $\mathbf{z} \in \mathbb{R}^{n_u+m}$  the dual variable associated with the bound constraints linked to  $\mathbf{w} = (\mathbf{u}, \mathbf{s})$ . The IPM solves the following unconstrained problem:

$$\min_{\mathbf{u}, \mathbf{s}} \psi_\mu(\mathbf{w}; \mathbf{y}) := L_\rho(\mathbf{u}, \mathbf{s}; \mathbf{y}) + B_\mu(\mathbf{u}, \mathbf{s}), \quad (15)$$

with  $B_\mu(\cdot)$  the barrier term

$$\begin{aligned} B_\mu(\mathbf{u}, \mathbf{s}) = & -\mu \sum_{i=1}^{n_u} (\log(u_i - u_i^b) + \log(u_i^\sharp - u_i)) \\ & - \mu \sum_{i=1}^m (\log(s_i - s_i^b) + \log(s_i^\sharp - s_i)). \end{aligned} \quad (16)$$

Introducing  $W = \llbracket \mathbf{w} \rrbracket$  and  $Z = \llbracket \mathbf{z} \rrbracket$ , the first-order optimality conditions of (15) are

$$\begin{cases} \nabla L_\rho(\mathbf{w}; \mathbf{y}) - \mathbf{z} = 0 \\ WZ - \mu \mathbf{e} = 0. \end{cases} \quad (17)$$

The IPM algorithm solves iteratively the system of nonlinear equations (17) with a Newton method. Along the iterations, the barrier term  $\mu$  is driven to 0 to recover the first-order conditions of the original AL subproblem (12).

2) *Solving the KKT system*: By applying the Newton method to the first-order conditions (17), the descent direction  $\mathbf{d} = (\mathbf{d}_w, \mathbf{d}_z)$  is computed directly as a solution of the nonsymmetric linear system

$$\begin{bmatrix} \nabla^2 L_\rho & -I \\ Z & W \end{bmatrix} \begin{bmatrix} \mathbf{d}_w \\ \mathbf{d}_z \end{bmatrix} = - \begin{bmatrix} \nabla L_\rho(\mathbf{w}; \mathbf{y}) - \mathbf{z} \\ WZ - \mu \mathbf{e} \end{bmatrix}. \quad (18)$$

Eliminating the last block row in (18), the descent  $\mathbf{d}_w$  is

$$[\nabla^2 L_\rho + \Sigma] \mathbf{d}_w = -\nabla_{\mathbf{w}} \psi_\mu(\mathbf{w}, \mathbf{y})^\top, \quad (19)$$

with the diagonal matrix  $\Sigma = W^{-1}Z$ . Once  $\mathbf{d}_w$  computed with (19), we recover the dual descent direction with  $\mathbf{d}_z = \mu W^{-1} \mathbf{e} - \mathbf{z} - \Sigma \mathbf{d}_w$ . To solve the linear system (19) efficiently, we exploit the structure of the AL's Hessian (14) with a Schur-complement approach.

**Proposition 3** (Schur complement). *The linear system (19) is equivalent to solving*

$$\begin{cases} S_{\mathbf{u}\mathbf{u}} \mathbf{d}_u = -\nabla_{\mathbf{u}} \psi_\mu^\top + \rho \nabla_{\mathbf{u}} c^\top [\Sigma_s + \rho I]^{-1} \nabla_{\mathbf{s}} \psi_\mu^\top \\ \mathbf{d}_s = [\Sigma_s + \rho I]^{-1} (-\nabla_{\mathbf{s}} \psi_\mu^\top + \rho (\nabla_{\mathbf{u}} c) \mathbf{d}_u), \end{cases} \quad (20)$$

where  $S_{\mathbf{u}\mathbf{u}}$  is the Schur-complement of the lower right block of the matrix  $[\nabla^2 L_\rho + \Sigma]$ :

$$S_{\mathbf{u}\mathbf{u}} = H_{\mathbf{u}\mathbf{u}} + \Sigma_u + \rho (\nabla_{\mathbf{u}} c)^\top (1 - \rho [\Sigma_s + \rho I]^{-1}) \nabla_{\mathbf{u}} c. \quad (21)$$

By using Proposition 3, we observe that the slack descent direction  $\mathbf{d}_s$  depends linearly on the control descent direction  $\mathbf{d}_u$ . Instead of factorizing the regularized Hessian matrix  $\nabla^2 L_\rho + \Sigma$  (with dimension  $(n_u + m) \times (n_u + m)$ ), we only have to factorize the Schur complement matrix (21) (with dimension  $n_u \times n_u$ ): the complexity becomes independent of the number of constraints in the problem.

Note that with an inertia-controlling algorithm, we can control  $\Sigma$  to ensure a positive definite matrix  $\nabla^2 L_\rho + \Sigma$ . It follows that  $S_{uu}$  is positive definite [19, Theorem 7.7.7, p.495]. Thus, the Schur-complement matrix can be factorized efficiently with a dense Cholesky factorization; readily available on GPUs.

3) *Static OPF algorithm*: The static OPF algorithm implements a typical AL algorithm, as presented in [18], [20]. The most expensive step is the resolution of the subproblems with IPM (all other operations are only involving vector or scalar operations). We adapt the IPM algorithm to our AL context. At each iteration  $k$ , we warmstart the IPM algorithm with the previous primal-dual solutions  $(\mathbf{w}_{k-1}, \mathbf{z}_{k-1})$ . The initial barrier is chosen according to [21], which decreases significantly the IPM iterations when we are close to the optimal solution.

The AL algorithm has two main bottlenecks: (i) its convergence is only linear [18] (ii) at a new iterate  $\mathbf{u}$  there is no guarantee that there exists a corresponding state  $\mathbf{x}$  (the Jacobian  $\nabla_{\mathbf{x}} g$  can be singular if we leave the power flow domain). In future work we will alleviate (i) with a refinement step [22], and (ii) can be safeguarded by computing the maximum step in the line-search procedure with bifurcation analysis [23].

### C. Real-time optimal power flow

Like the static OPF algorithm, the real-time OPF algorithm is also derived from the AL formulation (12). Our real-time OPF algorithm follows the method introduced in [7], and does not use an active-step procedure as in [2].

In this subsection, we assume that the problem is parameterized by a time index  $t \in \mathbb{N}$ , corresponding to varying load conditions  $(\mathbf{p}_t^d, \mathbf{q}_t^d)$ :

$$\min_{\mathbf{u}, \mathbf{s}} f_t(\mathbf{u}) + \mathbf{y}^\top (c_t(\mathbf{u}) - \mathbf{s}) + \frac{\rho}{2} \|c_t(\mathbf{u}) - \mathbf{s}\|^2. \quad (22)$$

To avoid an expensive explicit solution for (22) for each time  $t$ , we track a suboptimal solution by reiterating the following procedure. We initiate at time  $t = 0$  the real-time algorithm with an optimal solution  $\mathbf{w}_0^* = (\mathbf{u}_0^*, \mathbf{s}_0^*)$  (for instance computed with the static OPF algorithm introduced in Section IV-B). Then, for all time  $t$ , we update the primal-dual variables  $(\mathbf{w}_t, \mathbf{y}_t)$  as follows

- 1) For new loads  $(\mathbf{p}_t^d, \mathbf{q}_t^d)$ , compute the gradient  $\mathbf{g}_t = \nabla_{\mathbf{w}} L_{\rho, t}(\mathbf{w}_t, \mathbf{y}_t)$  and the Hessian  $H_t = \nabla_{\mathbf{w}\mathbf{w}}^2 L_{\rho, t}(\mathbf{w}_t, \mathbf{y}_t)$
- 2) Solve the bounded quadratic problem (QP) and update the primal variable  $\mathbf{w}_{t+1}$  with the solution

$$\min_{\mathbf{w}} \mathbf{g}_t^\top (\mathbf{w} - \mathbf{w}_t) + \frac{1}{2} (\mathbf{w} - \mathbf{w}_t)^\top H_t (\mathbf{w} - \mathbf{w}_t) \quad (23)$$

s.t.  $\mathbf{w}^b \leq \mathbf{w} \leq \mathbf{w}^\#$ ,

- 3) Set  $\mathbf{y}_{t+1} = \mathbf{y}_t + \rho(c_t(\mathbf{u}_{t+1}) - \mathbf{s}_{t+1})$

Step (1) can be evaluated efficiently using the reduced space procedure we introduced in Section III. The QP problem (23) can be solved efficiently with an IPM method.

Indeed, the problem (23) presents the same structure as the original AL subproblem (12). That means that in practice, we can solve (23) with IPM, using the same Schur-complement procedure introduced in Proposition 3. As the Hessian is constant, most of the time is spent factorizing the Schur-complement matrix in the IPM algorithm.

## V. NUMERICAL RESULTS

We now implement the reduction presented in Section III, and use the implementation to solve the static OPF and real-time OPF presented in Section IV. We detail the implementation we are using in Section V-A. Then, the two algorithms are tested respectively in Section V-B and Section V-C.

### A. Implementation

The two algorithms introduced in Section IV have two main blocks: the computation of the dense reduced Hessian (14), and the factorization of the (dense) Schur-complement matrix (21). Both operations are amenable to GPU accelerators, leading us to an entirely GPU accelerated implementation in the programming language Julia publicly available<sup>1</sup>.

1) *Implementing the callbacks on the GPU*: Based on the algorithm laid out in Section III-C

- *Kernels*: we use the portability layer KernelAbstractions.jl to implement the objective  $f(\cdot)$ , the power flow  $g(\cdot)$ , and the constraints  $c(\cdot)$ , so we can evaluate all functions using vectorization on the GPU.
- *Automatic differentiation*: we have developed a custom GPU backend to compute the first and second-order sensitivities of the kernels  $f(\cdot), g(\cdot), c(\cdot)$
- *Sparse linear system*: all the sparse linear systems in §III-B are solved using the LU refactorization solver `cusolverRF`. The sparsity pattern associated with the power flow's Jacobians  $\nabla_{\mathbf{x}} g$  is static, as defined by the network topology. Hence, we factorize the Jacobian during the presolve and transfer the factorization to the device. Every new Jacobian  $\nabla_{\mathbf{x}} g$  is refactorized directly on the GPU, without any data host-device transfer. With the Jacobian refactorized, `cusolverRF` is able to solve the linear system with multiple right-hand-sides, in batch. Together with our custom AD GPU backend, it enables us to accumulate the reduced Hessian in one shot using batched parallel Hessian-vector products (9).
- *Power flow solver*: the power flow equations are solved with the Newton-Raphson algorithm (4), entirely on the GPU. We stop the algorithm once:  $\|g(\mathbf{x}_k, \mathbf{u})\|_2 < 10^{-10}$ .

2) *Porting the optimization algorithms to the GPU*: As discussed in Section IV, the IPM algorithm is the core component both for the static OPF and for the real-time OPF algorithms. Here, we use the MadNLP solver [24], written entirely in Julia. We modify MadNLP to wrap the GPU

<sup>1</sup><https://github.com/exanauts/ExaPF-Opt>

callbacks. To that end, MadNLP takes the reduced Hessian — computed on the GPU as described in §V-A1 — assembles the Schur-complement (21) with cuBLAS, and then applies the Cholesky factorization of cuSOLVER. All that procedure happens entirely on the GPU, without any data transfer to the host.

3) *Benchmark library*: We test the static and the real-time OPF algorithms on three different instances from the PGLIB library [25], depicted in Table I. We run all experiments with a NVIDIA V100 GPU (with 32GB RAM), using CUDA 11.3.

Case	$n_v$	$n_e$	$n_x$	$n_u$	$m$
PEGASE1354	1,354	1,991	2,447	519	5,337
PEGASE2869	2,869	4,582	5,227	1,019	12,034
PEGASE9241	9,241	16,049	17,036	2,889	41,340

TABLE I  
CASE INSTANCES OBTAINED FROM PGLIB

### B. Static optimal power flow

We test the static OPF algorithm presented in §IV-B on the three instances in Table II. In the stopping criterion, we set  $\eta_{primal} = 10^{-5}$  and  $\eta_{dual} = 10^{-4}$ . The results are presented in Table II (the reference objective  $f^*$  and computation time  $t_{ref}$  are computed by solving the original OPF problem (1) with Ipopt+MA27 and PowerModels.jl [26]). We observe that we are able to recover Ipopt’s solution, with good accuracy. The algorithm takes many iterations to converge, leading to total running time being an order of magnitude greater than Ipopt (on case9241pegase, Ipopt converges in only 60s). However, our algorithm remains tractable, and is a net improvement comparing to previous implementation of the reduced space methods [10].

We detail in Figure 1 the convergence of the algorithm on case1354pegase. The algorithm converges in 369 iterations. The IPM algorithm is restarted 18 times in the AL routine, to update the penalty  $\rho$  and the multiplier  $\mathbf{y}$  (thus explaining the peaks in the evolution of the dual feasibility). As we increase the penalty  $\rho$ , the primal infeasibility decreases linearly. The second plot depicts the evolution of the maximum relative violation for each operational constraints (in p.u). We observe that in practice the evolution of the infeasibility depends on the scaling used for the different constraints (§IV-A2): the greater the scaling  $\sigma_{c,i}$  is, the faster the infeasibility of the constraint  $i$  will be driven to 0.

Case	$f$	$(f - f^*)/f^*$	$t_{ref}$ (s)	Time AL (s)	#it	Time/it (s)
PEGASE1354	$7.4069287 \times 10^4$	$9.2 \times 10^{-7}$	2.5	48.	369	0.13
PEGASE2869	$1.3399920 \times 10^5$	$6.7 \times 10^{-7}$	6.3	134.	427	0.31
PEGASE9241	$3.1591213 \times 10^5$	$3.4 \times 10^{-6}$	60.	1495.	672	2.22

TABLE II  
PERFORMANCE OF THE STATIC OPF ALGORITHM.

### C. Real-time optimal power flow

We test the real-time OPF algorithm presented in §IV-C. We suppose that the loads ( $\mathbf{p}_t^g, \mathbf{q}_t^g$ ) are varying along the time, and are updated at every minute. To model the evolution of the loads, we use the time-series provided by [27]: as illustrated in Figure 2, all loads drop suddenly by 20% at time  $t = 2$ ,

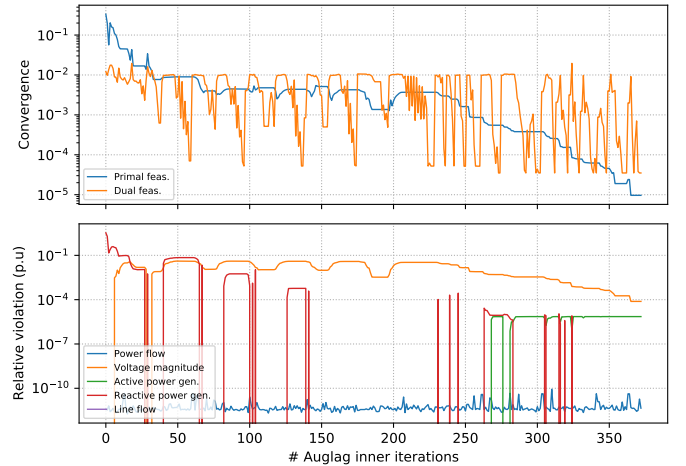


Fig. 1. Solving the static OPF for case1354pegase: the first plot displays the evolution of the primal and the dual infeasibility, and the second plot displays the evolution of the relative infeasibility for the different kind of operational constraints.

making it difficult to track the optimal solution. For all time  $t$ , the real-time algorithm should update the tracking control  $\mathbf{w}$  in a time-span  $\Delta t$ , with  $\Delta t \ll 1\text{mn}$ .

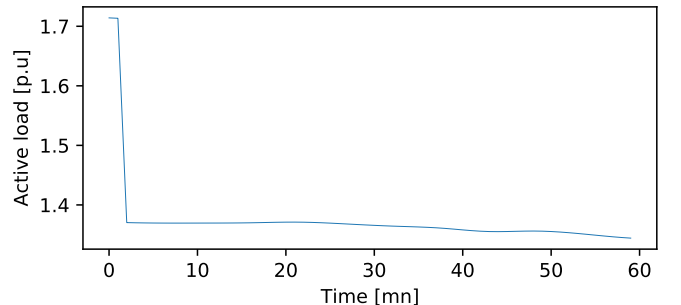


Fig. 2. Evolution of the active load at bus 1 for case1354pegase.

At time  $t = 0$ , the initial primal-dual solution ( $\mathbf{w}_0, \mathbf{y}_0$ ) is computed using the static OPF algorithm. For all time  $t$ , we use our GPU implementation to update the tracking point. This operation involves two expensive operations: (i) computing the reduced Hessian for the new load conditions ( $\mathbf{p}_t^d, \mathbf{q}_t^d$ ) (ii) solving the bounded QP problem (23). We detail in Table III the time spent inside these two operations: `LinAlg` is the time spent in the Cholesky solver (factorization and triangular solve). `Eval` is the time spent in the QP callbacks (involving only BLAS operations). We observe that it takes less than one second to update the tracking point for case1354pegase and case9241pegase, slightly longer for case9241pegase.

We now assess the effectiveness of the tracking algorithm. In Figure 3, we control case1354pegase every minute, during one hour. At time  $t = 2$ , the perturbation happens and the loads drop by 20%. The real-time algorithm is able to recover a suboptimal solution in 15 minutes (at  $t > 17$ , the relative gap with Ipopt’s objective is less than  $2 \times 10^{-4}$ , with

Case	Hess (s)	#it	QP resolution			$\Delta t$ (s)
			LinAlg. (s)	Eval. (s)	Tot (s)	
PEGASE1354	0.06	12	0.005	0.014	0.08	0.14
PEGASE2869	0.16	12	0.096	0.029	0.16	0.32
PEGASE9241	1.6	14	0.187	0.200	3.0	3.6

TABLE III

TIME TO UPDATE THE TRACKING POINT (IN SECONDS).

a primal infeasibility for the operational constraints closes to  $1 \times 10^{-2}$ ). The third plot, displaying the absolute difference between  $p_t^g$  and the optimal point  $p_t^{g,*}$ , shows that the median deviation in active power generations is less than  $1 \times 10^2$ .

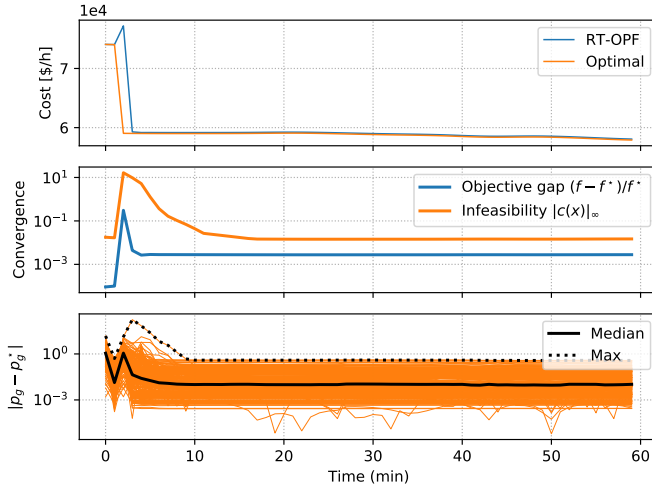


Fig. 3. Tracking the AC-OPF solution of case1354pegase with the RT-OPF algorithm. The first and the second plots display respectively (i) the operating costs computed respectively with the real-time OPF and with Ipopt. (ii) the convergence of the real-time OPF. The third plot displays for each generator the absolute difference between Ipopt solution and real-time OPF's setpoint.

## VI. CONCLUSION

We have devised a feasible Augmented Lagrangian algorithm, whose iterates satisfy by design the physical equations of the power network. A GPU implementation of the reduced space algorithm has proven to be critical for its tractability. On the one hand, we have shown that the algorithm is effective at solving large-scale static OPF problem and, to the best of our knowledge, is the first reduced space algorithm able to solve case9241pegase with second-order information. On the other hand, the reduced space algorithm is able to track a suboptimal solution in a real-time OPF setting, and can adapt quickly to large variations in the loads.

Future work will optimize the algorithm by intertwining more closely the IPM algorithm with the Augmented Lagrangian algorithm with the expectation of more accurate solutions, in less iterations.

## REFERENCES

- [1] F. Capitanescu, "Critical review of recent advances and further developments needed in AC optimal power flow," *Electric Power Systems Research*, vol. 136, pp. 57–68, Jul. 2016. [Online]. Available: <https://doi.org/10.1016/j.epsr.2016.02.008>
- [2] Y. Tang, K. Dvijotham, and S. Low, "Real-time optimal power flow," *IEEE Transactions on Smart Grid*, vol. 8, no. 6, pp. 2963–2973, 2017.
- [3] L. Gan and S. H. Low, "An online gradient algorithm for optimal power flow on radial networks," *IEEE Journal on Selected Areas in Communications*, vol. 34, no. 3, pp. 625–638, 2016.
- [4] A. Hauswirth, A. Zanardi, S. Bolognani, F. Dörfler, and G. Hug, "Online optimization in closed loop on the power flow manifold," in *2017 IEEE Manchester PowerTech*. IEEE, 2017, pp. 1–6.
- [5] E. Dall'Anese and A. Simonetto, "Optimal power flow pursuit," *IEEE Transactions on Smart Grid*, vol. 9, no. 2, pp. 942–952, 2016.
- [6] H. Dommel and W. Tinney, "Optimal Power Flow Solutions," *IEEE Transactions on Power Apparatus and Systems*, vol. PAS-87, no. 10, pp. 1866–1876, Oct. 1968.
- [7] V. M. Zavala and M. Anitescu, "Real-time nonlinear optimization as a generalized equation," *SIAM Journal on Control and Optimization*, vol. 48, no. 8, pp. 5444–5467, 2010.
- [8] N.-Y. Chiang, R. Huang, and V. M. Zavala, "An augmented lagrangian filter method for real-time embedded optimization," *IEEE Transactions on Automatic Control*, vol. 62, no. 12, pp. 6110–6121, 2017.
- [9] S. Frank, I. Steponavice, and S. Rebennack, "Optimal power flow: a bibliographic survey I: Formulations and deterministic methods," *Energy Systems*, vol. 3, no. 3, pp. 221–258, Sep. 2012. [Online]. Available: <http://link.springer.com/10.1007/s12667-012-0056-y>
- [10] J. Kardos, D. Kourounis, and O. Schenk, "Reduced-space interior point methods in power grid problems," *arXiv preprint arXiv:2001.10815*, 2020.
- [11] M. B. Cain, R. P. O'neill, A. Castillo *et al.*, "History of optimal power flow and formulations," *Federal Energy Regulatory Commission*, vol. 1, pp. 1–36, 2012.
- [12] W. F. Tinney and C. E. Hart, "Power flow solution by newton's method," *IEEE Transactions on Power Apparatus and systems*, no. 11, pp. 1449–1460, 1967.
- [13] Z. Wang, I. M. Navon, F.-X. Le Dimet, and X. Zou, "The second order adjoint analysis: theory and applications," *Meteorology and atmospheric physics*, vol. 50, no. 1, pp. 3–20, 1992.
- [14] R. T. Rockafellar, "Augmented lagrangians and applications of the proximal point algorithm in convex programming," *Mathematics of operations research*, vol. 1, no. 2, pp. 97–116, 1976.
- [15] D. P. Bertsekas, "Multiplier methods: a survey," *Automatica*, vol. 12, no. 2, pp. 133–145, 1976.
- [16] A. Wächter and L. T. Biegler, "On the implementation of an interior-point filter line-search algorithm for large-scale nonlinear programming," *Mathematical programming*, vol. 106, no. 1, pp. 25–57, 2006.
- [17] E. G. Birgin and J. M. Martínez, *Practical augmented Lagrangian methods for constrained optimization*. SIAM, 2014.
- [18] J. Nocedal and S. J. Wright, *Numerical optimization*, 2nd ed., ser. Springer series in operations research. New York: Springer, 2006, oCLC: ocm68629100.
- [19] R. A. Horn and C. R. Johnson, *Matrix analysis*. Cambridge university press, 2012.
- [20] A. R. Conn, G. Gould, and P. L. Toint, *LANCELOT: a Fortran package for large-scale nonlinear optimization (Release A)*. Springer Science & Business Media, 2013, vol. 17.
- [21] D. Ma, D. Orban, and M. A. Saunders, "A Julia implementation of Algorithm NCL for constrained optimization," *arXiv preprint arXiv:2101.02164*, 2021.
- [22] E. G. Birgin and J. M. Martínez, "Improving ultimate convergence of an augmented lagrangian method," *Optimization Methods and Software*, vol. 23, no. 2, pp. 177–195, 2008.
- [23] I. Dobson, "Computing a closest bifurcation instability in multidimensional parameter space," *Journal of nonlinear science*, vol. 3, no. 1, pp. 307–327, 1993.
- [24] S. Shin, C. Coffrin, K. Sundar, and V. M. Zavala, "Graph-based modeling and decomposition of energy infrastructures," *arXiv preprint arXiv:2010.02404*, 2020.
- [25] S. Babaeinejadsarookolae, A. Birchfield, R. D. Christie, C. Coffrin, C. DeMarco, R. Diao, M. Ferris, S. Fliscounakis, S. Greene, R. Huang *et al.*, "The power grid library for benchmarking ac optimal power flow algorithms," *arXiv preprint arXiv:1908.02788*, 2019.
- [26] C. Coffrin, R. Bent, K. Sundar, Y. Ng, and M. Lubin, "Powermodels.jl: An open-source framework for exploring power flow formulations," in *2018 Power Systems Computation Conference (PSCC)*. IEEE, 2018, pp. 1–8.
- [27] Y. Kim and M. Anitescu, "A real-time optimization with warm-start of multiperiod ac optimal power flows," *Electric Power Systems Research*, vol. 189, p. 106721, 2020.

The submitted manuscript has been created by UChicago Argonne, LLC, Operator of Argonne National Laboratory (“Argonne”). Argonne, a U.S. Department of Energy Office of Science laboratory, is operated under Contract No. DE-AC02-06CH11357. The U.S. Government retains for itself, and others acting on its behalf, a paid-up nonexclusive, irrevocable worldwide license in said article to reproduce, prepare derivative works, distribute copies to the public, and perform publicly and display publicly, by or on behalf of the Government. The Department of Energy will provide public access to these results of federally sponsored research in accordance with the DOE Public Access Plan. <http://energy.gov/downloads/doe-public-access-plan>.